



**HAL**  
open science

## Inverse modeling of annual atmospheric CO<sub>2</sub> sources and sinks: 2. Sensitivity study

Philippe Bousquet, P. Peylin, Philippe Ciais, M. Ramonet, P. Monfray

### ► To cite this version:

Philippe Bousquet, P. Peylin, Philippe Ciais, M. Ramonet, P. Monfray. Inverse modeling of annual atmospheric CO<sub>2</sub> sources and sinks: 2. Sensitivity study. *Journal of Geophysical Research: Atmospheres*, 1999, 104 (D21), pp.26179-26193. 10.1029/1999JD900341 . hal-02923861

**HAL Id: hal-02923861**

**<https://hal.science/hal-02923861>**

Submitted on 28 Oct 2020

**HAL** is a multi-disciplinary open access archive for the deposit and dissemination of scientific research documents, whether they are published or not. The documents may come from teaching and research institutions in France or abroad, or from public or private research centers.

L'archive ouverte pluridisciplinaire **HAL**, est destinée au dépôt et à la diffusion de documents scientifiques de niveau recherche, publiés ou non, émanant des établissements d'enseignement et de recherche français ou étrangers, des laboratoires publics ou privés.

# Inverse modeling of annual atmospheric CO<sub>2</sub> sources and sinks

## 2. Sensitivity study

P. Bousquet,<sup>1</sup> P. Peylin, P. Ciais, M. Ramonet, and P. Monfray

Laboratoire des Sciences du Climat et de l'Environnement, Gif sur Yvette, France

**Abstract.** Atmospheric transport models can be used to infer surface fluxes of atmospheric CO<sub>2</sub> from observed concentrations using inverse methods. One of the main problem of these methods is the question of their sensitivity to all the parameters involved in the calculation. In this paper we study precisely the influence of the main parameters on the net CO<sub>2</sub> fluxes inferred by an annual Bayesian three-dimensional (3-D) inversion of atmospheric CO<sub>2</sub> monthly concentrations. This inversion is described as the control inversion ( $S_0$ ) of Bousquet *et al.* [this issue]. Successively, at regional to global spatial scales we analyze the numerical stability of the solution to initial fluxes and errors, the influence of a priori flux scenario, the sensitivity to the atmospheric transport model used, the influence of  $\delta^{13}\text{C}$  measurements, and the influence of the atmospheric network. We find that the atmospheric transport model introduces a large uncertainty to the inferred budget, which overcomes our control run uncertainties. The effects of vertical transport on CO<sub>2</sub> concentrations appear to be a critical point that has to be investigated further. Spatial patterns of fluxes also have significant influence on a regional basis. We notice that accounting for the Baltic Sea station (BAL) deeply modifies the Europe versus Asia partition of the land uptake at mid and high latitudes of the Northern Hemisphere. We also analyze the weak influence of using  $\delta^{13}\text{C}$  measurements as additional constraints. In the tropics we find that the low level of constraints imposed by the atmospheric network limits the analysis of fluxes to zonal means. Finally, we calculate overall estimates of CO<sub>2</sub> net sources and sinks at continental scale, accounting for all sensitivity tests. Concerning the controversial partition of CO<sub>2</sub> sink at mid and high latitudes of the Northern Hemisphere, we find (on average, for the 1985-1995 period) an overall partition of the sink of  $0.7\pm 0.7$  Gt C yr<sup>-1</sup> for North America,  $0.2\pm 0.3$  Gt C yr<sup>-1</sup> for the North Pacific Ocean,  $0.5\pm 0.8$  Gt C yr<sup>-1</sup> for Europe,  $0.7\pm 0.3$  Gt C yr<sup>-1</sup> for the North Atlantic Ocean, and  $1.2\pm 0.8$  Gt C yr<sup>-1</sup> for north Asia. This overall partition tends to place an important land uptake over north Asia. However, uncertainties remain large when we account for all the sensitivity tests.

## 1. Introduction

Global atmospheric observations of CO<sub>2</sub> concentration in the atmosphere can be converted into net surface fluxes by using atmospheric transport models. In order to determine a set of surface fluxes that best matches the atmospheric measurements, inverse methodologies are currently being used [Enting *et al.*, 1995; Ciais *et al.*, 1995a, Hein *et al.*, 1996; Rayner *et al.*, 1997]. Inversions are based on mass balance calculations [Law *et al.*, 1996; Bousquet *et al.*, 1996] or are of synthesis type [Enting *et al.*, 1993]. Bousquet *et al.* [this issue] use the latter approach in order to calculate the CO<sub>2</sub> fluxes exchanged over 11 continental regions and 8 ocean regions of the globe. Briefly, for each type of source involved in the CO<sub>2</sub> budget we establish a global map of a priori fluxes on a monthly basis. The sources (or sinks) are fossil fuel emissions (FOS), land use changes (DEF), land gross primary production (GPP), land total respiration (RES), land net uptake (BIO\_UPT), and net ocean fluxes (OCE). Each type of

source is divided into several source regions over the entire globe which thus determines the source base functions. Note that for land areas the number of source base functions is 3 times the number of source regions because we have three spatial and temporal patterns representing continental exchanges (GPP, RES, and BIO\_UPT). The model response for each source base function is computed with the TM2 three-dimensional model [Heimann, 1995]. The Bayesian inverse method optimizes annual source strengths using assumptions on (1) an a priori set of monthly fluxes and errors, (2) the model responses for each source base function, and (3) the monthly atmospheric measurements and errors that are being assimilated to constrain the sources and the sinks regionally.

In this paper we examine how robust the inferred fluxes of our control inversion ( $S_0$ ) are to these three types of assumptions in the inverse procedure. To do so, first, we perform a detailed sensitivity analysis to the a priori settings. This includes a sensitivity analysis of the inversion to the initial source strengths and initial errors on the sources prescribed to the model. We also study the way to choose different a priori geographical patterns of emission versus uptake within a given source region and how the increase or decrease the number of regions does impact the inferred sources magnitudes. Second, we address the effect of using another transport model (the TM3 model) instead of the TM2 model in the inverse procedure. This test of atmospheric transport is particularly important since model intercomparisons

<sup>1</sup>Also at Université de Versailles Saint Quentin en Yvelines, Versailles, France

have already revealed potentially large differences in the CO<sub>2</sub> concentration fields that are simulated by different transport codes, highlighting, among others, strong interactions between the seasonal variability of vertical mixing and of land biospheric emissions [Denning *et al.*, 1995, 1997]. Third, we evaluate the specific constraints that are added to the inferred fluxes when <sup>13</sup>C/<sup>12</sup>C isotope ratio measurements are included in addition to CO<sub>2</sub> concentration measurements. Also, the specific influence of using in the inversion the CO<sub>2</sub> records obtained at continental stations, on board ship cruises, and over the air column by aircraft is examined. The influence of each station is also studied. Finally, a synthesis discussion of the 14 sensitivity tests is given in section 5.

All the net fluxes inferred in the sensitivity tests are summarized in Table 1 for five continental regions and four oceanic regions from test  $S_0$ , which corresponds to our control inversion (see Bousquet *et al.* [this issue], hereinafter referred as B99), to test  $S_{14}$ . These nine regions correspond to a spatial scale that is hereinafter referred to as the "continental and ocean basin" scale.

## 2. Sensitivity to a Priori Fluxes and Errors

### 2.1. Numerical Stability to Initial Fluxes Values

We perform a sensitivity test to evaluate the influence of initial conditions on the solution inferred by the inverse procedure. To do so, we modify the a priori values of gross and net fluxes using a random number generator. This generator provides a multiplying factor for initial fluxes between 0.7 and 1.3. Thus we introduce a  $\pm 30\%$  random "noise" to the initial a priori values. Fifty inversions are done successively. For BIO\_UPT flux we do not set a priori values to 0.0 Gt C yr<sup>-1</sup> for each region as in the control inversion  $S_0$  (see Bousquet *et al.* [this issue]) but we use a priori values given by Friedlingstein *et al.* [1995].

The a posteriori CO<sub>2</sub> fluxes do not differ from  $S_0$  by more than  $\pm 0.1$  Gt C yr<sup>-1</sup> over each region considered, except for the

deforestation source over South America which departs from  $S_0$  by 0.3 Gt C yr<sup>-1</sup> in one of the 50 test runs. We conclude from that test that the solution of  $S_0$  is globally stable against the a priori flux estimate. This stability was expected because the inverse problem is over constrained (as discussed by B99). However, in the tropics a weak state of constraints appears in this sensitivity test which justifies the need to aggregate all biospheric fluxes in the tropics to present the inversion results: land uptake (BIO\_UPT) and deforestation (DEF).

### 2.2. Numerical Stability to Initial Errors

The choice of the initial errors on the fluxes is a key point in Bayesian inverse methods. In our a priori flux scenario (see B99, section 3), these errors are set to reasonable values for GPP, RES, FOS, and DEF, given our present knowledge of the carbon cycle. For OCE and BIO\_UPT we choose large values so as not to nudge the solution to the prior estimates. This choice is arbitrary, and it is important to evaluate its influence on the inferred budget. To do so, we perform a test in which the a priori errors for the land uptake (BIO\_UPT) range from  $\pm 0.1$  to  $\pm 10$  Gt C yr<sup>-1</sup> per source base function, errors on other fluxes being taken as in the standard inversion  $S_0$ . We recall that in  $S_0$  we set errors on the flux BIO\_UPT to  $\pm 1.5$  Gt C yr<sup>-1</sup> for nontropical regions and to  $\pm 0.5$  Gt C yr<sup>-1</sup> for tropical ones, with the a priori flux magnitude for BIO\_UPT being set to zero. Therefore, in the extreme case when initial errors tend to zero, the inferred biospheric fluxes also tend to zero over nontropical land areas. Figure 1 plots the inferred net biospheric flux as a function of initial errors ( $\Sigma$ ) in the Northern Hemisphere and in the tropics. When the initial error value is increased from 0 to 10, the inferred fluxes are able to change and may relax toward an asymptotic value. The more rapidly the asymptotic value is reached, the stronger is the constraint imposed by the atmospheric network.

In the Northern Hemisphere, we observe two different behaviors (Figure 1a). The optimized fluxes over North America and Europe are stable within  $\pm 0.1$  Gt C yr<sup>-1</sup> for  $\Sigma > \pm 0.4$  Gt C yr<sup>-1</sup>,

**Table 1.** Net Fluxes for 14 Sensitivity Tests From  $S_1$  to  $S_{14}$

	$S_0$	$S_1^*$	$S_2^*$	$S_3^*$	$S_4$	$S_5$	$S_6$	$S_7$	$S_8$	$S_9$	$S_{10}$	$S_{11}$	$S_{12}$	$S_{13}$	$S_{14}$
<i>Land Uptake</i>															
Arctic	0,2	0,1	0,2	0,2	-0,4	0,1	0,0	0,2	-0,3	0,3	0,2	0,1	0,1	0,1	-
North America	-0,5	-0,6	-0,8	-0,8	-1,0	-1,0	-0,4	-0,3	-1,1	-0,5	-0,4	-0,5	-0,5	-1,0	-0,8
Europe	-0,3	-0,5	-0,5	-0,6	-1,5	-0,2	-0,3	-0,7	-0,2	-0,4	-0,1	-0,3	-0,3	-0,3	-0,8
North Asia	-1,5	-1,5	-1,5	-1,5	-0,4	-1,3	-1,7	-1,0	-0,9	-1,6	-1,5	-1,3	-1,4	-0,5	-
South of 30°N	1,0	0,5	0,4	0,3	0,9	1,1	1,4	0,6	0,3	0,9	0,2	1,0	0,9	0,3	0,2
Total	-1,2	-2,0	-2,2	-2,4	-2,4	-1,2	-1,0	-1,2	-2,1	-1,3	-1,5	-1,0	-1,1	-1,4	-1,4
<i>Ocean Uptake</i>															
North pacific	-0,3	-0,2	-0,1	-0,1	0,2	-0,3	-0,1	-0,5	0,0	-0,1	-0,3	-0,2	-0,2	-0,3	-
North Atlantic	-0,8	-0,8	-0,8	-0,7	-0,1	-0,7	-0,8	-0,8	-0,5	-0,7	-0,8	-0,7	-0,7	-0,5	-0,8
15°N-15°S	0,6	0,5	0,6	0,6	0,4	0,6	0,5	0,6	0,6	0,3	0,6	0,0	0,2	0,6	0,5
15°S-90°S	-1,0	-1,0	-1,0	-1,0	-0,8	-1,1	-1,4	-0,9	-0,7	-1,0	-0,9	-1,0	-0,9	-0,9	-0,8
Total	-1,5	-1,5	-1,3	-1,2	-0,2	-1,6	-1,8	-1,6	-0,7	-1,5	-1,4	-1,8	-1,7	-1,1	-1,1

In Gt C yr<sup>-1</sup>.  $S_0$  is the control run from B99.  $S_1$ ,  $S_2$  and  $S_3$  represent inversions performed using  $\delta^{13}\text{C}$  measurements as additional constraints. In  $S_4$  we use TM3 transport model instead of TM2. In  $S_5$ , no explicit land uptake pattern is considered. In  $S_6$ , the ocean scenario of Aumont [1998] is used instead of that of Takahashi *et al.* [1997]. Continental influenced monitoring sites have been removed in  $S_7$  (TM2) and  $S_8$  (TM3). In  $S_9$ , Pacific cruise data (P01 to P16) have been removed for the inversion. In  $S_{10}$  China Sea cruise data have been removed for the inverse calculation. In  $S_{14}$ , Arctic region has been aggregated with North American one, north Asian with European, and North Pacific with North Atlantic.

\*Performed for 1990-1995 period only.

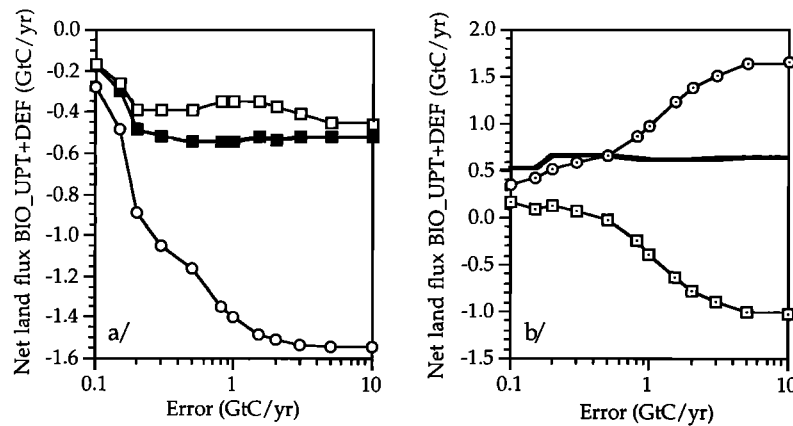


**Figure 1.** (a) Nontropical and (b) tropical net land flux at continental scale (BIO\_UPT+DEF). For North America (solid squares), Europe (open squares) and north Asia (open circles) in Figure 1a and for tropical America (dotted squares), tropical Africa, and tropical Asia (dotted circles) and the sum of the two previous curves (solid line) in Figure 1b.

meaning that for  $\Sigma$  above  $\pm 0.4 \text{ Gt C yr}^{-1}$ , the inferred flux is not altered by the initial guess. In contrast, the inferred flux over northern Asia depends on the first guess estimate for  $\Sigma < \pm 1.1 \text{ Gt C yr}^{-1}$ . This latter flux therefore requires larger a priori errors to relax to its asymptotic value, probably because it is less constrained by atmospheric observations than the other two. The arbitrary choice of  $\pm 1.5 \text{ Gt C yr}^{-1}$  for the initial errors on this region in the control run  $S_0$  is thus relevant considering the fact that we want to limit the influence of initial conditions for regions where fluxes are highly uncertain. Including in the inversion some recent atmospheric measurements over Siberia [Sugawara *et al.*, 1997] could reduce the uncertainties on the inferred fluxes over that domain. It is worth noting that uptake over North America does not correlate with uptake over Siberia when the value of  $\Sigma$  is increased (Figure 1a), suggesting that the present set of atmospheric observations is sufficient to separate both areas, with North America (and Europe) being better determined than northern Asia.

In the tropics the inferred flux over South America strongly anticorrelates with the one over Africa and Asia, when the value of  $\Sigma$  increases (Figure 1b). Over both regions an asymptotic value is not approached until  $\Sigma > \pm 3.0 \text{ Gt C yr}^{-1}$ . Yet, the sum of all tropical land fluxes is rather constant within  $\pm 0.1 \text{ Gt C yr}^{-1}$  for  $\Sigma > \pm 0.5 \text{ Gt C yr}^{-1}$ . This reveals the poor level of constraint fluxes at a continental scale in the tropics, where only a zonal average estimate can be safely inferred. Thus in run  $S_0$ , setting the value of  $\Sigma$  to  $\pm 0.5 \text{ Gt C yr}^{-1}$  in the tropics is appropriate to produce an unbiased zonal land flux estimate, but the longitudinal partitioning of tropical land fluxes shall not be discussed.

### 2.3. Influence of the a Priori Flux Scenario Patterns

Our choice to optimize net CO<sub>2</sub> fluxes over large continental and ocean regions assumes that spatial patterns are fixed in the a priori fluxes within each region. In order to test the influence of the a priori flux scenario on the result of the inversion, we have performed three sensitivity studies where we modified the spatial patterns or the spatial discretisation of initial fluxes.

**2.3.1. Spatial discretization (number of source regions).** In order to test the influence of source regions in the inversion we have performed five different model inversions based on a decreasing number of source regions used to optimize the surface fluxes. The maximum number of source regions is 34 (66 source

base functions), corresponding to 16 land fluxes (48 source base functions, see B99), 14 ocean sources, three deforestation sources and one fossil source (Table 2). We decrease progressively the number of source regions down to nine regions (14 source base functions) consisting of three land fluxes (nine source base functions), three ocean fluxes, one deforestation source, and one fossil source (Table 2). All these inversions ( $S_{11}$  to  $S_{14}$ ) are referred to XXbio\_YYoce with XX standing for the number of source regions representing land fluxes and YY standing for the number of source regions representing ocean fluxes. In that case, the name of "11bio\_8oce" corresponds to the control inversion  $S_0$ . One may anticipate that a larger number of source regions allow for more degrees of freedom and relax the effect of observational constraints.

When the number of source regions decreases from  $S_{11}$  to  $S_{14}$ , the ocean uptake decreases from 1.8 to 1.1  $\text{Gt C yr}^{-1}$ , while conversely, the land uptake increases from 1.0 to 1.4  $\text{Gt C yr}^{-1}$  (Table 3). This trade-off between ocean and land absorption is not entirely symmetric because fossil fuel emissions are also reduced, which explains why the total BIO\_UPT + OCE is not constant in Table 3. We verify in this test that an increasing number of regions correlate with a smaller reduction in the uncertainty estimates of the inferred fluxes. This effect can be explained because increasing the number of source regions means reducing the constraint imposed by atmospheric measurements.

**Table 2.** Description of the Space Discretization of the Inversions Used for the Sensitivity Test

	GPP, RES, BIO_UPT	OCE	DEF	FOS	Total
16bio_14oce	48	14	3	1	66
13bio_11oce	39	11	3	1	54
11bio_8oce	33	8	3	1	45
6bio_5oce	18	5	3	1	27
3bio_3oce	9	3	1	1	14

Number of source base functions for the inverse procedure. "Bio" stands for land fluxes and "oce" stands for ocean fluxes. Each inversion is referred as XXbio\_YYoce where XX is the number of regions for land fluxes (it has to be multiplied by 3 to have the number of source base functions). YY is the number of ocean regions.

**Table 3.** Net Fluxes and Errors for Five Configurations of the Inversion Using Decreasing Number of Source Base Functions

	$S_{11}$		$S_{12}$		$S_{13}$		$S_0$		$S_{14}$		
	16bio_14oce		13bio_11oce		11bio_8oce		6bio_5oce		3bio_3oce		
<b>Land uptake</b>											
Arctic	0,1	± 0,3	0,1	± 0,3	0,2	± 0,3	0,1	± 0,2	-	-	-
North America	-0,5	± 0,5	-0,5	± 0,5	-0,5	± 0,6	-1,0	± 0,4	-0,8	± 0,4	
Europe	-0,3	± 0,9	-0,3	± 0,9	-0,3	± 0,8	-0,3	± 0,6	-0,8	± 0,4	
North Asia	-1,3	± 0,7	-1,4	± 0,7	-1,5	± 0,7	-0,5	± 0,4	-	-	-
South of 30°N	1,0	± 1,3	0,9	± 1,2	1,0	± 1,0	0,3	± 0,9	0,2	± 0,6	
<b>Total</b>	<b>-1,0</b>	<b>± 1,8</b>	<b>-1,1</b>	<b>± 1,8</b>	<b>-1,1</b>	<b>± 1,6</b>	<b>-1,4</b>	<b>± 1,2</b>	<b>-1,4</b>	<b>± 0,8</b>	
<b>Ocean uptake</b>											
North Pacific	-0,2	± 0,3	-0,2	± 0,3	-0,3	± 0,2	-0,3	± 0,2	-0,8	± 0,3	
North Atlantic	-0,7	± 0,3	-0,7	± 0,3	-0,8	± 0,3	-0,5	± 0,3	-	-	-
15°S-15°N	0,0	± 0,4	0,2	± 0,3	0,6	± 0,2	0,6	± 0,1	0,5	± 0,1	
90°S-15°S	-1,0	± 0,4	-0,9	± 0,4	-1,0	± 0,3	-0,9	± 0,3	-0,8	± 0,2	
<b>Total</b>	<b>-1,8</b>	<b>± 0,7</b>	<b>-1,7</b>	<b>± 0,7</b>	<b>-1,5</b>	<b>± 0,5</b>	<b>-1,1</b>	<b>± 0,4</b>	<b>-1,1</b>	<b>± 0,4</b>	

In Gt C yr<sup>-1</sup>. "Bio" stands for net land uptake (BIO\_UPT+DEF) and "oce" stands for ocean uptake. The sum of BIO\_UPT and OCE is not constant because fossil fuel emissions are modified.

The results of the three inversions 16bio\_14oce, 13bio\_11oce, and 11bio\_8oce differ markedly one from another in the tropics (Table 3). The ocean equatorial source even drops to zero in run 16bio\_14oce, which has four distinct ocean regions in the tropics. This is rather unrealistic regarding direct estimates of the fluxes [Andrie *et al.*, 1986; Boutin and Eicheto, 1997; Metzl *et al.*, 1995].

When the number of regions is increased jointly with a reduction of the tropical sea-to-air flux, a stronger land source is inferred so that the sum of all tropical fluxes is conserved within 0.4 Gt C yr<sup>-1</sup>. This suggests that tropical fluxes are poorly constrained not only over land regions but also over some ocean regions, including those containing a measurement site (GMI, ASC, SEY, Pacific Ocean cruises). The atmospheric circulation in the tropics generates a couplet between rather weak horizontal zonal winds and strong vertical motion in the rising branch of the Hadley cells [Heimann and Keeling, 1989], which may qualitatively explain why a tropical sea level station has less spatial representativeness than a midlatitude one.

When the number of regions is reduced compared to  $S_0$  settings, in runs 6bio\_5oce and 3bio\_3oce, a correlation appears between the flux estimates of North America and Eurasia. The North American sink is 2 times larger than in  $S_0$  and the Eurasian uptake is abated accordingly. This solution is more in agreement with Fan *et al.*'s [1998] results even if North America remains smaller than in their study. In the 3bio\_3oce case the inferred solution is nudged by the small number of degrees of freedom. The solution for the average Northern Hemisphere land uptake differs significantly between runs 6bio\_5oce and 3bio\_3oce compared to  $S_0$  but remains stable if the number of regions becomes larger than in  $S_0$ .

Overall, using too many degrees of freedom leads to having numerous flux estimates that give a good fit at monitoring sites, whereas using too few degrees of freedom tends to nudge the solution and provides a poor fit to the observations. In both cases the validity of the inferred solution is doubtful, especially for poorly constrained regions. The possibility of using many more

degrees of freedom using an adjoint model approach is still under investigation [Kaminski *et al.*, 1997]. The choice of 11bio\_8oce as the reference inversion appears as a good compromise between these two limitations.

**2.3.2. Land spatial patterns of the prior sources within each region.** In the sensitivity run  $S_5$ , we test an alternative solution to represent land uptake (BIO\_UPT) within each region used for inverse calculation. This is obtained by adjusting the sum of gross primary production (GPP) and total respiration (RES) over each region. In other words, we do not use the explicit land uptake component (BIO\_UPT) as in our control inversion  $S_0$ . The sums of RES and GPP for each region are set to zero in the prior estimate and are associated with error bars equal to those assigned to BIO\_UPT in  $S_0$ . The results are listed in Table 1. At the global scale the fluxes inferred for  $S_5$  are similar to those obtained in  $S_0$  within 0.2 Gt C yr<sup>-1</sup>. However, the North American sink is increased by a factor of 2 in  $S_5$  compared to  $S_0$  and reaches up to 1.0±0.6 Gt C yr<sup>-1</sup>. Concomitantly, the Eurasian sink decreases by 0.3 Gt C yr<sup>-1</sup>, and the terrestrial source in the tropics increases by 0.2 Gt C yr<sup>-1</sup>. We conclude from this that important modifications in the optimized sources and sinks can occur at a continental scale in response to changing the prior spatial regional patterns of land uptake. We further investigated the case of North America to determine which region (temperate / boreal) is responsible for a more pronounced uptake in  $S_5$  compared to  $S_0$ . In  $S_5$ , the flux apportionment between boreal and temperate America is of +0.4 Gt C yr<sup>-1</sup> in the boreal zone (source) against -1.4 Gt C yr<sup>-1</sup> in the temperate region (sink). In contrast,  $S_0$  produces a more even distribution of the sink, with boreal North America being a small source of 0.1 Gt C yr<sup>-1</sup> and temperate North America being a sink of 0.6 Gt C yr<sup>-1</sup>. The overall increase in the North American sink between  $S_0$  and  $S_5$  is a direct effect of changes in prior spatial patterns: in  $S_0$  we use the Friedlingstein *et al.* [1995] flux pattern that has proportionally more flux and spatial structures in the boreal ecosystems (compared to temperate or tropical ones) than GPP or RES have. Changes in the boreal versus temperate partition

suggests that these two regions are not well constrained separately in the inverse procedure. In fact, only two stations (KEY and SBL) are located close and downwind of the eastern coast of North America, other sites being either continental (NWR, UTA) or situated on the west North American coast (CMO, OPW, CSJ).

**2.3.3. Ocean spatial patterns of the prior sources within each region.** In this section we perform an inversion  $S_6$  that differs from  $S_0$  by the use of an alternative air-to-sea CO<sub>2</sub> flux field. The test inversion  $S_6$  uses as a priori the monthly global sea-to-air fluxes distribution calculated by Aumont [1998] from the three dimensional (3-D) ocean carbon model (Institut Pierre Simon Laplace, IPSL) based on general ocean circulation model OPA7-NPZD [Delecluse et al., 1993; Six and Maier-Reimer, 1996]. The results of that inversion ( $S_6$ ) indicate a marked increase of the global ocean sink, on the order of 0.4 Gt C yr<sup>-1</sup> compared to  $S_0$ , whereas the global land uptake is abated by the same amount (Table 1). The change between  $S_0$  and  $S_6$  is caused primarily by an increase in the Southern Ocean CO<sub>2</sub> uptake from 1.0 to 1.4 Gt C yr<sup>-1</sup>. This is attributed to the existence of different spatial patterns in the two sets of prior air-to-sea fluxes from Takahashi et al. [1997] and Aumont [1998] over the southern ocean. Takahashi et al., [1997] do not have strong longitudinal gradients in the sea-to-air fluxes, since the  $\Delta p\text{CO}_2$  measurements that they have used are rather scarce south of 40°S to constrain their extrapolation method. In the model study of Aumont, [1998], limited areas of strong outgassing occur within the band 40°S -60°S and create a complex longitudinal structure, possibly as an artifact of the ocean model simulation (O. Aumont, personal communication, 1997).

The existence of such localized source areas, sometimes close to measurement sites, can partly offset the uptake of CO<sub>2</sub> by subtropical and sub-Antarctic surface waters that is inferred from the existing monitoring sites and can force the inverse procedure to infer a larger sink in the whole latitude band in order to match the atmospheric observations. One of these sources is located in the sub-Antarctic Indian Ocean and therefore influences the Amsterdam Island site (AMS), Cape Grim (CGO), and Baring Head station (BHD). Table 1 also shows that tropical regions are a net source to the atmosphere of 1.4 Gt C yr<sup>-1</sup> (+0.4 Gt C yr<sup>-1</sup> compared to  $S_0$ ), while the Northern Hemisphere land uptake shifts from 2.1 Gt C yr<sup>-1</sup> in  $S_0$  to 2.4 Gt C yr<sup>-1</sup> in  $S_6$ . Thus the meridional distribution of the terrestrial carbon uptake is adjusted (decrease in the tropics and increase in the north) in order to compensate for the ocean effect noticed above (increase in the south and small decrease in the north).

**2.3.4. Discussion.** For both changes in land and ocean uptake spatial patterns, one can notice that the smaller the spatial scale is, the more significant the changes are. At global and hemispheric scales the inverse problem is constrained enough to almost give the same inferred fluxes with all the patterns we have tested. However, at regional or continental scales, differences reach 0.5 Gt C yr<sup>-1</sup> (a factor of 2 for North America sink) but remain compatible with error bars of  $S_0$ . Concerning space discretization of fluxes, it appears that it is difficult to increase the number of regions in the tropics without modifying significantly the CO<sub>2</sub> budget at continental scale.

With these tests we see that spatial patterns of initial sources become important at the scale used to make the spatial discretization and the inverse calculation. So, as mentioned by Peylin et al. [1999] it may be important to discuss inferred fluxes at a spatial scale larger than the calculation scale. As atmospheric network density increases, one can attempt to adjust more closely

the space discretization in order to limit its influence on inferred fluxes while keeping a good state of constraint. A coherence has to be found between atmospheric constraint, model resolution, and space and time discretization of fluxes. However, if one wants to increase the number of regions (over the continents of the Northern Hemisphere, for instance) by a large factor, the computing cost of the response functions becomes a problem. One possible solution to this issue is to use an adjoint model to calculate source base function for all pixels of the transport model and make a posteriori spatial rearrangements [Kaminski et al., 1997].

Another important point is the time discretization of fluxes. In our approach, we run monthly flux fields in the transport model, but we only optimize annual fluxes (against monthly averaged observations) in the inverse procedure. As most atmospheric data are provided on a weekly or a monthly base, the method could be adapted to optimize monthly fluxes. This would increase the degrees of freedom by a factor of 12. The study of the influence of time discretisation on optimized fluxes in an important issue [Peylin et al., 1999].

### 3. Influence of Atmospheric Transport

As recently shown, one main source of uncertainties in the results of atmospheric CO<sub>2</sub> inversions appears to be the modeled atmospheric transport [Law et al., 1996; Denning et al., 1997]. Inversion  $S_4$  (Table 1) is performed with the same characteristics as  $S_0$  but uses the TM3 transport model [Heimann, 1995] instead of TM2. The TM3 model is based on the same wind fields as TM2 but has finer vertical (19 sigma levels instead of 9) and horizontal (4° x 5° instead of 7.5° x 7.5°) resolution. The same source base functions as in inversion  $S_0$  are run in model TM3, and the outputs are used in the standard inverse procedure. The flux solution of  $S_4$  exhibits major differences from  $S_0$ . The net land uptake of CO<sub>2</sub> is multiplied by a factor of 2 (2.4 Gt C yr<sup>-1</sup>) whereas the ocean uptake drops down to 0.2 Gt C yr<sup>-1</sup>. Over the continents, the sink in North America increases from 0.5±0.6 up to 1.0±0.4 Gt C yr<sup>-1</sup>. The European sink is multiplied by a factor of 5 (1.5±0.5 Gt C yr<sup>-1</sup>), whereas the sink over northern Asia is reduced from 1.5±0.7 to 0.4±0.4 Gt C yr<sup>-1</sup>.

Such large differences between the results of  $S_0$  and  $S_4$  are mainly due to the rectifier effect of atmospheric concentrations that is present in the TM3 model (see B99, section 2). This effect contributes to the increase of the annual mean modeled CO<sub>2</sub> concentration over the Northern Hemisphere continents with respect to the marine boundary layer concentrations. This is especially true at European “continental” sites such as BAL, SCH, WES, or TAP. The continent-to-ocean CO<sub>2</sub> concentration gradients predicted by TM3 are larger than the one for TM2 or for the observations. As a consequence, the inferred sink over Northern Hemisphere continents is much larger for the modeled concentrations to match the observed ones. This is especially true over Europe where more continental sites can be found. Another consequence of the TM3 rectifier is that the global ocean uptake drops to 0.2 Gt C yr<sup>-1</sup> in order for the sum of global land plus ocean fluxes to match atmospheric trend. As a result, the Northern Hemisphere oceans are no longer a significant net sink in  $S_4$ , as compared to  $S_0$ . This result is doubtful as the North Atlantic has been determined to be a significant net sink [Lefèvre, 1995; Takahashi et al., 1997]. Finally, it is interesting to observe that the differences between TM3 and TM2 almost vanish in the tropics. The continental fluxes south of 30°N and the ocean

fluxes south of 15°N are changed by  $< 0.2 \text{ Gt C yr}^{-1}$  in  $S_4$  as compared to  $S_0$ .

The partitioning of the Northern Hemisphere carbon flux over land seems to be overestimated in TM3, which may reflect a model overestimate of the continental concentrations because of the “rectifier” effect. In this context there is a problem of coherence between the treatment of continental sites in the TM3 model (no selection of continental data according to wind speed and direction or any other criterion) and the subsampling of CO<sub>2</sub> data at continental stations that are most of the time selected to remove some of the local sources influence. According to *Ramonet and Monfray* [1996] a model presenting a higher horizontal and vertical resolution is more sensitive to subscale processes such as local meteorological effects or regional environmental effects (presence of a forest, of factories, etc.). The TM3 model has a better horizontal and vertical resolution than TM2 and should therefore provide a more realistic representation of the atmospheric transport than TM2. To improve the coherence between model and selected data, we have to improve the representation of continental sites in the model and to test vertical subgrid scale mixing parametrizations (convection and diffusion).

## 4. Influence of Atmospheric Measurements

### 4.1. Influence of CO<sub>2</sub> Atmospheric Network

**4.1.1. Individual site influence.** The first test we have performed is a bootstrap test. The principle is to remove each site one by one from the station list and to compare the results of all the inversions calculated with 76 sites instead of 77 to the standard inversion  $S_0$ . For each region we compute the difference of inferred net flux between the inversion performed without station XXX and  $S_0$ . We keep differences when they are greater than  $0.1 \text{ Gt C yr}^{-1}$  for one given region. Only three stations induce differences larger than  $0.1 \text{ Gt C yr}^{-1}$ .

First, removing Baltic station (BAL) changes deeply the partition of the Northern Hemisphere land uptake: Europe becomes a sink of  $1.1 \text{ Gt C yr}^{-1}$  ( $0.3$  in  $S_0$ ) while the sink over north Asia is reduced to  $0.8 \text{ Gt C yr}^{-1}$  ( $1.5$  in  $S_0$ ). The sink over North America is only reduced by  $0.1 \text{ Gt C yr}^{-1}$ . This impressive result is probably due to a bad representation of BAL station by a model like TM2 that has a coarse horizontal resolution. BAL flasks are taken over the Baltic Sea whose extension in longitude is of the order of magnitude of one grid box of TM2. BAL is very high in CO<sub>2</sub> in the data on annual average (see B99, Figure 4). Thus, if we do not use it, the inverse calculation increases the sink over Europe that was limited by the presence of BAL. Consequently, the sinks over north Asia and North America are reduced. One can notice that the North American sink is much less reduced than the north Asiatic sink. Actually, the total Eurasian land uptake is only modified by  $0.2 \text{ Gt C yr}^{-1}$  by this test.

Then, removing the UUM Mongolian station induces an increase of  $0.2 \text{ Gt C yr}^{-1}$  for the north Asiatic land uptake ( $-1.7$  instead of  $-1.5$ ). UUM is a site located high above sea level and is also probably not well represented by the model. Finally, removing Sable Island station (SBL) increases the North American sink by  $0.2 \text{ Gt C yr}^{-1}$  ( $-0.7$  instead of  $-0.5$ ). SBL is a bit high in CO<sub>2</sub> compared to what the model predicts. If we do not use it the inverse procedure has a tendency to increase the north American sink. In conclusion, except for BAL site, other stations have a small individual impact on the results of our control inversion  $S_0$ .

**4.1.2. Continental sites.** The present CO<sub>2</sub> atmospheric

network is the most important network for trace gas measurements. However, its density is highly variable geographically. Some regions have many monitoring sites (Europe, for instance) and some other regions have no sites at all (South America and Siberia, for instance). Most of the sites are marine boundary layer sites. However, 10 sites located inland or under land influence have been added to our control inversion  $S_0$ . As a sensitivity test, we have removed these 10 sites from the inverse calculation (BAL, WES, SCH, CIM, NWR, UTA, RYO, TAP, QPC, KSN). This test is performed for both TM2 ( $S_7$ ) and TM3 ( $S_8$ ) models.

For TM2, net land uptake and net ocean uptake are almost unchanged compared to  $S_0$  ( $\pm 0.2 \text{ Gt C yr}^{-1}$ ). Note, however, that in this test the fraction of the biospheric sink located in the mid and high latitudes of the Northern Hemisphere is reduced by 15% and drops to  $1.8 \text{ Gt C yr}^{-1}$  ( $2.1 \text{ Gt C yr}^{-1}$  in  $S_0$ ). In contrast, important changes occur for TM3 model. Removing sites under continental influence leads to increase the global ocean uptake by  $0.5 \text{ Gt C yr}^{-1}$  and to decrease the land uptake by  $0.4 \text{ Gt C yr}^{-1}$ . The Northern Hemisphere land uptake is reduced by 30% compared to the standard TM3 inversion ( $S_4$ ). The decrease of the land uptake over 15°N in both TM2 and TM3 can be explained by the reduction of continent to ocean gradients caused by the exclusion of continental sites in  $S_7$  and  $S_8$ . The decrease is twice as important in TM3 than in TM2 because the continent to ocean contrasts of a priori modeled atmospheric concentrations are much larger in TM3 due to a stronger rectifier effect.

One can also notice a significant balance of net land uptake between north Asia and Europe for both models. In the TM2 inversion ( $S_7$ ), the north Asia sink is reduced to  $1.0 \text{ Gt C yr}^{-1}$  and the European sink is increased to  $0.7 \text{ Gt C yr}^{-1}$ . This effect is coherent with the individual influence of BAL station noticed above. In the TM3 inversion ( $S_8$ ), the north Asia sink is increased up to  $0.9 \text{ Gt C yr}^{-1}$  and the European sink is reduced to  $0.2 \text{ Gt C yr}^{-1}$ . It is interesting to note that if both models agree on the amplitude of the uptake over Siberia, there is no agreement between the amplitude of European and North America land uptakes. The sink is located preferentially over North America for TM3 and over north Asia for TM2.

Using mainly marine boundary layer sites in inversions  $S_7$  and  $S_8$  should remove most of the influence of the rectifier effect that is present in TM3. However, the two models still fail to converge to the same partition of fluxes for the Northern Hemisphere. This means that atmospheric transport is a major source of uncertainties in inverse studies at all spatial scales. Moreover, as long as there is no precise quantification of the rectifier effect above continents, there is no way to reduce the uncertainty due to transport models. The quantification of the rectifier effect remains an open and major question that will have to be addressed in the near future if one wants to use transport models for atmospheric inversions. The third phase of the TRANSCOM experiment should go in this direction (TRANSCOM is an international model intercomparison experiment that has been running since 1994; see *Law et al.* [1996] and *Denning et al.* [1997]).

**4.1.3. Cruise data influence.** In  $S_0$  we use two sets of atmospheric data built from marine cruises in the Pacific Ocean (P01 to P16) and in the China sea (C01 to C07). In order to see the influence of these data that have been aggregated per latitude band, two inversions are performed without them.

In  $S_9$ , Pacific cruise data are removed from the inverse calculation. One can see on Table 1 that changes concerning net land uptake stay below  $0.1 \text{ Gt C yr}^{-1}$  between  $S_9$  and  $S_0$ .

Nevertheless, ocean uptake is modified at the hemispheric scale. The contrast between Northern Hemisphere ocean sink and equatorial source is reduced by 0.6 Gt C yr<sup>-1</sup> when compared to  $S_0$ : Equatorial source is reduced by 0.3 Gt C yr<sup>-1</sup> whereas Northern Hemisphere sink is also reduced by 0.3 Gt C yr<sup>-1</sup>. In the tropics, Pacific cruise data present higher CO<sub>2</sub> concentrations than other stations of the same latitude band (+0.2 to +1.2 ppm). North of 15°N, the situation is the opposite with Pacific cruises presenting lower CO<sub>2</sub> concentrations than other stations of the same latitude band. Removing Pacific cruises from the inverse calculation thus implies that a smaller tropical source and a smaller midlatitude sink are needed to match the observations.

In  $S_{10}$ , South China Sea cruises have been removed from inverse calculation (C01 to C07). In our control inversion  $S_0$ , tropical Asia is found to be a source of 0.8±0.4 Gt C yr<sup>-1</sup>. This estimate drops to 0.2±0.4 Gt C yr<sup>-1</sup> in test  $S_{10}$  (Table 1). China Sea data which have been aggregated into seven stations that are close to China and Southeast Asia exhibit CO<sub>2</sub> concentrations 0.5 to 2.0 ppm higher on average than other stations at the same latitude over the central Pacific Ocean. As a consequence, the inverse procedure places a substantial source over tropical Asia between 10°S and 30°N to fit these stations. This source is reduced by 60% without these sites. The Northern Hemisphere land uptake is also reduced by 15%. Note, however, that north Asia land uptake is unchanged in  $S_{10}$  when compared to  $S_0$ .

**4.1.4. Japanese flight data influence.** Vertical profiles of CO<sub>2</sub> have been already used to test the vertical transport in atmospheric models [Monfray *et al.*, 1996]. As most of CO<sub>2</sub> fluxes are exchanged at the surface, aircraft measurements can give an integrated view of the exchange of carbon. It is interesting to quantify the influence of these data on the results of the inversion. To do so, we have performed an inversion without data from the Japanese vertical profile. No significant changes in net fluxes were noted at global and continental scales (test not reported in Table 1). However, within north Asia we note a balance of the net land uptake between boreal Asia and temperate Asia. In  $S_0$ , boreal Asia has a sink of 0.6 Gt C yr<sup>-1</sup> and temperate Asia has a sink of 0.9 Gt C yr<sup>-1</sup>, whereas without the Japanese profiles the partition is the opposite. This test shows that the Japanese vertical profile is important to constraining the partition of land uptake at a regional scale within the Asian continent.

**4.1.5. Calibration issue.** In inversion  $S_0$ , data from different atmospheric network are aggregated together to increase the constraints on the surface fluxes. The intercalibration problem between these networks is still not completely resolved even if a lot of work has already been done by flask exchange campaigns between laboratories involved in atmospheric CO<sub>2</sub> measurements. Tanks containing calibration gas are exchanged between more than 10 groups (every 4 years). Our group is also involved in a flask exchange program with Division of Atmospheric Research (CSIRO/DAR, Australia) and National Oceanographic and Atmospheric Administration Climate Monitoring and Diagnostic Laboratory (NOAA/CMDL, United States Of America) at the Cape Grim station (CGO). However, some measurement groups are still not involved in such exchange programs. This limits the use of their stations in inverse procedures.

We perform an inversion where annual means of all data from NOAA CMDL network are increased by 0.25 ppmv (test not reported in Table 1). This value is in the range of intercalibration problem as suggested by NOAA CMDL group (K.A. Masarie, personal communication, 1998). The results of the inverse procedure are modified by < 0.1 Gt C yr<sup>-1</sup> at continental scale.

However, the global offset for CO<sub>2</sub> concentrations that we optimize in the inverse procedure is increased by 0.2 ppmv compared to  $S_0$  offset. This change can be explained by the fact that NOAA CMDL network represents the largest network (80%). Thus the inverse procedure preferentially modifies the offset instead of the regional fluxes.

We have performed two other sensitivity tests in which we increase by 0.5 ppmv the concentrations of the stations either of the IPSL Laboratoire des Sciences du Climat et de l'Environnement (MHT, AMS) or of the CSIRO DAR (CGO, CG4, CG6, BHD, MAQ, MAW). For the IPSL LSCE network the main change is a limited decrease of 0.2 Gt C yr<sup>-1</sup> of the sub-Antarctic subtropical sink. For the CSIRO DAR, the main differences with  $S_0$  is a small increase of the southern nontropical land net source of 0.2 Gt C yr<sup>-1</sup> and a small decrease of the equatorial ocean source of 0.1 Gt C yr<sup>-1</sup>. Effects for other regions remain under 0.1 Gt C yr<sup>-1</sup>.

## 4.2. Influence of δ<sup>13</sup>C Measurements

**4.2.1. Methodology.** The control inversion  $S_0$  is performed without using δ<sup>13</sup>C measurements. In this section the influence of adding δ<sup>13</sup>C measurements as an additional constraint to regional fluxes is studied. Methodology and specific formalism to include <sup>13</sup>C measurements as additional constraints on net CO<sub>2</sub> sources and sinks is described in the appendix. Roughly, δ<sup>13</sup>C can be expressed as a combination of the modeled responses of CO<sub>2</sub> source base functions and of the modeled responses of source base functions for the CO<sub>2</sub> gross fluxes (corresponding to disequilibrium terms). Each coefficient of this combination is the product (hereinafter called isoflux) of a CO<sub>2</sub> source strength and of an isotopic signature. Isoflux is linearized according to Tarantola [1987] and Hein *et al.* [1997] formulations. Thus, for δ<sup>13</sup>C we not only optimize net CO<sub>2</sub> annual flux strengths but also one isotopic signature per source.

We use δ<sup>13</sup>C measurements from 24 monitoring sites that have been progressively available since 1990 as part of the NOAA/CMDL air sampling program [Trolier *et al.*, 1996]. The reference period for this test is 1990-1995 to insure consistency between CO<sub>2</sub> and δ<sup>13</sup>C data. Over that period the global CO<sub>2</sub> rate of increase is 1.3±0.1 ppm yr<sup>-1</sup> and the global δ<sup>13</sup>C trend is set to -0.025‰ yr<sup>-1</sup>. The fossil source strength is assigned to 6.2±0.3 Gt C yr<sup>-1</sup>. Three different inversions are presented to examine the specific role of δ<sup>13</sup>C measurements:  $S_1$  has the same constraints as  $S_0$  (i.e., CO<sub>2</sub> measurements only) but covers the period 1990-1995,  $S_2$  is identical to  $S_1$  but includes the δ<sup>13</sup>C data and trend, and  $S_3$  is identical to  $S_2$  but the isotopic disequilibria and fluxes signatures are maintained to a fixed value (identical to the priors).

**4.2.2. Modeled δ<sup>13</sup>C.** Figure 2 compares the modeled δ<sup>13</sup>C values (a priori and optimized) at six stations of the NOAA CMDL network with the atmospheric observations. Figure 2 shows that the fit to the monthly δ<sup>13</sup>C observations is satisfying overall at all sites but is not as good as the fit obtained for CO<sub>2</sub> only. As for  $S_0$ , the  $S_1$  inversion that includes <sup>13</sup>C performs better for nontropical sites. The reasons of the inversion shortcoming in the tropics could be the same as that for CO<sub>2</sub> (poor constraint on the continental fluxes from the atmospheric stations) but could be also specific to δ<sup>13</sup>C (the crudeness of the ocean disequilibrium representation or absence of seasonality in the isotopic signatures). Figure 3 presents the simulated north to south annual δ<sup>13</sup>C concentrations at the monitoring sites. The inversion decreases the amplitude of the mean north to south

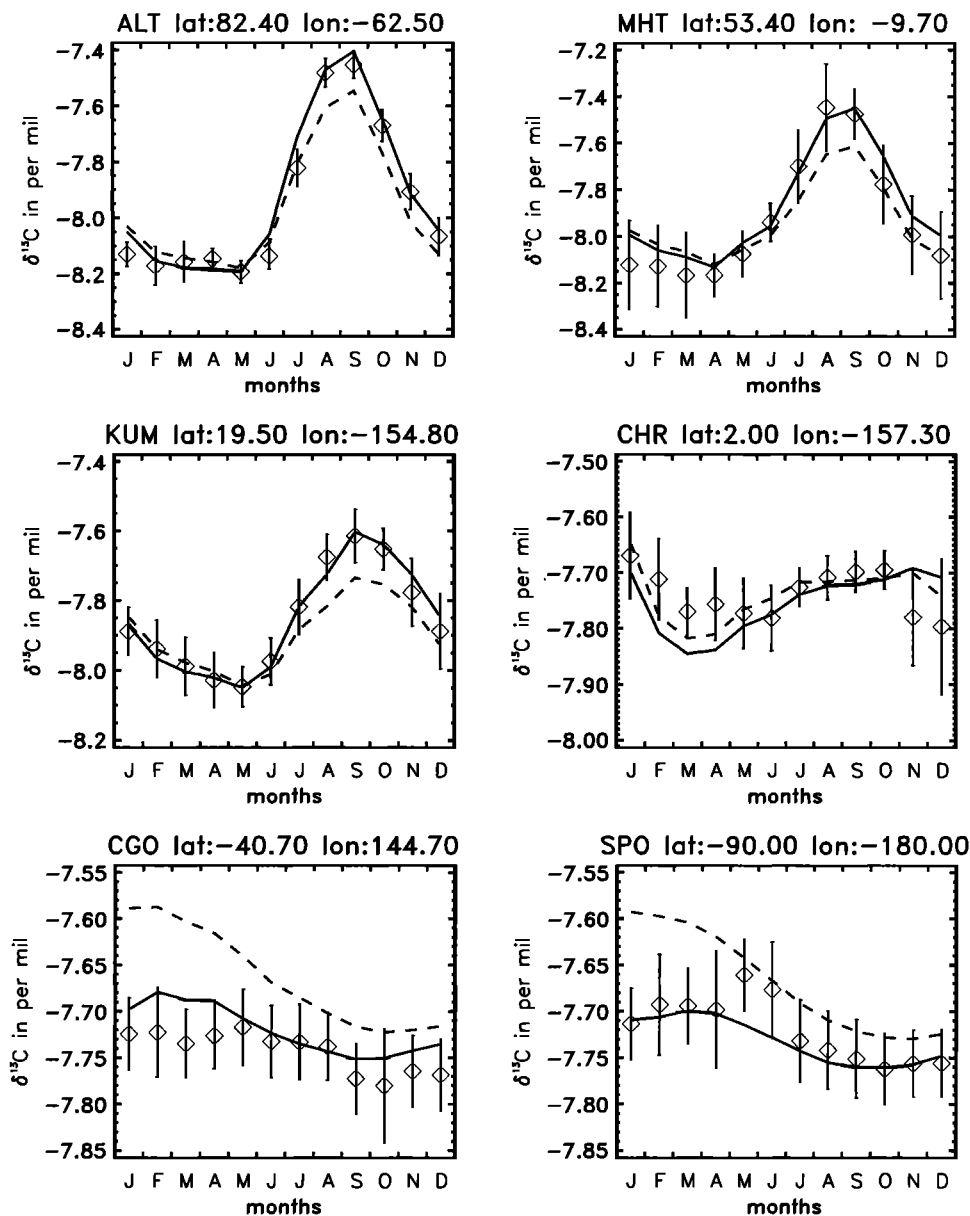


**Figure 2.** Modeled and observed  $\delta^{13}\text{C}$  concentrations for six monitoring sites used in inversion  $S_1$ . Dots stand for atmospheric data (one climatological year of observations averaged over the 1990-1995 period). Dashed line is for the a priori modeled concentrations. Solid line is for the optimized model concentrations.

$\delta^{13}\text{C}$  profile, which indicates a terrestrial uptake and matches rather closely the observed values at most of the sites.

**4.2.3. Inferred fluxes.** Table 4 presents the optimized net CO<sub>2</sub> fluxes and errors obtained respectively in  $S_1$ ,  $S_2$ , and  $S_3$  at the global and continental scale. Table 4 is a detailed version of Table 1 for inversions  $S_1$ ,  $S_2$ , and  $S_3$ . The results of  $S_1$  (only CO<sub>2</sub> data) differ slightly from those of  $S_0$  and show an increase of the Northern Hemisphere land uptake from 2.1 to 2.5 Gt C yr<sup>-1</sup>. Conversely, the continental tropical source is reduced from 1.0 to 0.5 Gt C yr<sup>-1</sup>. Such values are consistent with studies that have estimated a larger biospheric sink during the early 1990s than in the 1980s [Ciais et al., 1995b; Francey et al., 1995; Keeling et al., 1996]. Comparing the results of  $S_2$  and  $S_1$ , one can clearly see that using  $\delta^{13}\text{C}$  measurements does not induce major changes in the inferred net CO<sub>2</sub> fluxes. Resulting differences do not exceed  $\pm 0.1\text{Gt C yr}^{-1}$  at a continental scale. Only, a slight

reduction of errors, of the order of  $\pm 0.1\text{Gt C yr}^{-1}$ , is achieved over the Northern Hemisphere land areas when the  $\delta^{13}\text{C}$  constraint is included. This result, which is surprising considering the importance of  $\delta^{13}\text{C}$  measurements in previous studies [Ciais et al., 1995b; Enting et al., 1995], can be attributed to four main causes.

First, we only use 24 stations for  $\delta^{13}\text{C}$ , versus 80 for CO<sub>2</sub>. This difference clearly gives a lower weight of the  $\delta^{13}\text{C}$  data in the inverse procedure. Second, uncertainties on the monthly  $\delta^{13}\text{C}$  values constructed from the flask measurements are comparatively larger than for CO<sub>2</sub> (synoptic variability, analytical precision, and interannual variability). Third, we include some stations under strong continental influence in the inversion procedure (e.g., BAL, TAP, WES, or SCH). Thus CO<sub>2</sub> gradients between oceans (marine boundary layer sites) and continents are already a powerful constraint on the geographical

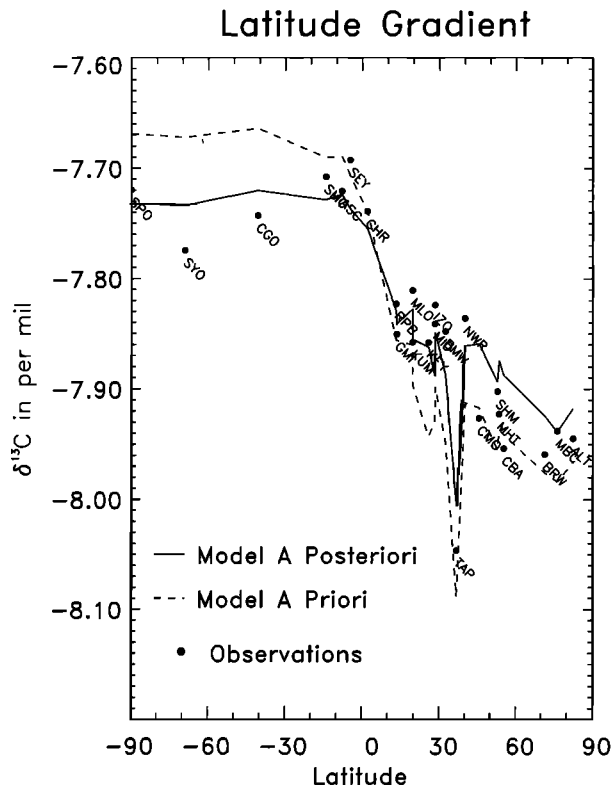


**Figure 3.** Modeled and observed  $\delta^{13}\text{C}$  north to south annual concentrations for six of the 24 monitoring sites used in inversion  $S_1$ . Dots stand for atmospheric data (one climatological year of observations averaged over the 1990-1995 period). Dashed line is for the a priori modeled concentrations. Solid line is for the optimized model concentrations.

partitioning of the fluxes. In this context,  $S_1$  yields a set of continental and ocean fluxes which is fully compatible with the  $\delta^{13}\text{C}$  information, in such a manner that adding  $\delta^{13}\text{C}$  in  $S_2$  does not change the inferred sources magnitude. Finally, one must consider that the inverse procedure based on  $\delta^{13}\text{C}$  optimizes the net fluxes, as well as the gross fluxes (via the disequilibria) and the isotopic signatures. This means that there could be a "temptation" for the inverse procedure to change the disequilibria or the isotopic signatures to match the  $\delta^{13}\text{C}$  constraint because these parameters are only constrained by the  $\delta^{13}\text{C}$  observations and not by the  $\text{CO}_2$  measurements. The changes inferred in the ocean disequilibrium are the only significant ones among all the parameters that are "determined" by  $\delta^{13}\text{C}$ . Biospheric disequilibrium is not significantly modified as it is linked to total respiration which is already constrained by  $\text{CO}_2$  measurements. Table 5 shows the a posteriori and a priori disequilibrium fluxes with the ocean for  $S_1$  and  $S_2$ . It indicates that the inverse procedure preferentially modifies the isotopic disequilibrium values to fit the  $\delta^{13}\text{C}$  data and especially the  $\delta^{13}\text{C}$  trend, which is a strong constraint on the inversion. In order to test this last hypothesis, we have performed an inversion  $S_3$  where we maintained all disequilibrium fluxes and isotopic signatures to their initial values by prescribing a very small error. In that case, the changes in the  $\text{CO}_2$  net fluxes are significantly more important in  $S_3$  than in  $S_2$ . For example, global land uptake increases by  $0.4 \text{ Gt C yr}^{-1}$  in  $S_3$  and only by  $0.1 \text{ Gt C yr}^{-1}$  in  $S_2$ .

In  $S_3$  the inversion procedure can only adjust the  $\text{CO}_2$  net exchange to fit  $\delta^{13}\text{C}$  data which enhances the influence of  $\delta^{13}\text{C}$  on the solution.

## 5. Summary and Discussion

In order to summarize the differences between each inversion and our control inversion  $S_0$ , we have calculated the  $\chi_m$  coefficient as the mean absolute difference between fluxes inferred in  $S_n$  ( $n$  represents the different tests) and fluxes inferred in  $S_0$  for the nine regions defined in Table 1 (see Figure 4).  $\chi_m$  are sorted and presented in a decreasing order. Figure 4 also plots the mean value of the a posteriori uncertainties at continental and ocean basin scale for all inversions which is  $\pm 0.4 \text{ Gt C yr}^{-1}$ . One can notice that all  $\chi_m$  remain below the mean a posteriori uncertainty except for run  $S_4$ , which corresponds to the use of the TM3 model. Modeled atmospheric transport is largely the most sensitive component of our study. The second most sensitive component is the influence of the spatial patterns given to the a priori fluxes ( $S_6$  and  $S_5$ ), especially for land uptake of  $\text{CO}_2$ . Then another sensible parameter is the use of continental sites that are not well represented in the model (such as BAL station).

The influence of each component depends on the spatial scale that is considered for the analysis. Changing the atmospheric transport model from two extreme behaviors with respect to the rectifier effect (TM2 and TM3) modifies the optimized fluxes and partitions between oceans and continents at all scales, from regional to global. This is a major limitation of current inverse modeling to constrain the regional carbon cycle, as mentioned in section 3. For all other tests the modifications on the inferred fluxes remain limited to regional and/or continental scales and remain most of the time within a posteriori uncertainties. Especially, some components such as flux uncertainties or number of source regions are very sensitive for poorly constrained regions like the tropical lands. We also see that the a posteriori fluxes at a continental scale (e.g., tropical America versus tropical Asia) depend critically on the a priori error given to the land fluxes. For poorly constrained regions like tropical continents, the zonal mean of fluxes is much better constrained

**Table 4.** Regional Results of the Inversions  $S_1$ ,  $S_2$  and  $S_3$

	$S_1$	$S_2$	$S_3$
Fossil fuel emissions	$6,2 \pm 0,3$	$6,1 \pm 0,3$	$6,1 \pm 0,3$
Continents	$-2,0 \pm 1,6$	$-2,2 \pm 1,5$	$-2,4 \pm 1,4$
Arctic	$0,1 \pm 0,3$	$0,2 \pm 0,3$	$0,2 \pm 0,3$
North America	$-0,6 \pm 0,6$	$-0,8 \pm 0,5$	$-0,8 \pm 0,4$
Europe	$-0,5 \pm 0,8$	$-0,5 \pm 0,7$	$-0,6 \pm 0,7$
North Asia	$-1,5 \pm 0,7$	$-1,5 \pm 0,6$	$-1,5 \pm 0,6$
South of 30°N *	$0,5 \pm 1,0$	$0,4 \pm 1,0$	$0,3 \pm 1,0$
Oceans	$-1,5 \pm 0,4$	$-1,3 \pm 0,5$	$-1,2 \pm 0,4$
North Pacific	$-0,2 \pm 0,2$	$-0,1 \pm 0,2$	$-0,1 \pm 0,2$
North Atlantic	$-0,8 \pm 0,3$	$-0,8 \pm 0,3$	$-0,7 \pm 0,3$
15°N-15°S	$0,5 \pm 0,1$	$0,6 \pm 0,1$	$0,6 \pm 0,1$
90°S-15°S	$-1,0 \pm 0,2$	$-1,0 \pm 0,2$	$-1,0 \pm 0,2$

In  $\text{Gt C yr}^{-1}$   $S_1$  is performed under the same conditions as  $S_0$  but for 1990-1995 period.  $S_2$  and  $S_3$  are two sensitivity runs using  $\delta^{13}\text{C}$  data as an additional constraint.

\* Deforestation and biospheric sink have been added in the tropics for both a priori fluxes and a posteriori fluxes. The reference period is 1990-1995.

**Table 5.** Oceanic Gross Fluxes and Isotopic Disequilibrium with the Ocean for  $S_2$  Inversion

	A priori	$S_2$
Gross ocean to atmospheric flux	86,6 ± 14,5	93,0 ± 11,5
North	2,1 ± 0,8	1,6 ± 0,8
North Pacific	10,5 ± 4,2	11,1 ± 4,2
North Atlantic (> 50°N)	4,2 ± 1,7	4,2 ± 1,7
North Atlantic (20-50°N)	5,5 ± 2,2	5,8 ± 2,2
Equator	19,0 ± 7,6	22,4 ± 4,8
20-50°S	24,8 ± 8,0	24,3 ± 5,7
Austral	20,5 ± 8,0	23,8 ± 7,3
Isotopic disequilibrium with oceans		
North Pacific	0,12 ± 0,2	0,12 ± 0,2
North Atlantic (> 50°N)	-0,50 ± 0,2	-0,50 ± 0,2
North Atlantic (20-50°N)	0,30 ± 0,2	0,34 ± 0,2
Equator	1,60 ± 0,2	1,70 ± 0,2
20-50°S	0,78 ± 0,2	-0,75 ± 0,2
90°-20°S	-0,50 ± 0,2	-0,58 ± 0,2

In Gt C yr<sup>-1</sup>.

than regional fluxes. Thus one should consider regrouping the regions to present relevant results.

Considering that the transport in nontropical areas is mainly driven by westerlies, one can reasonably believe that adding more measurement sites over some land areas like north Asia or South America is likely to improve the state of constraint on surface fluxes. The situation is more complex in the tropics due to the characteristics of the atmospheric circulation at these latitudes. Adding ground measurements to better constrain surface fluxes would not be as efficient as at midlatitudes because of the importance of the vertical transport between 15°N and 15°S. One good strategy may be to develop CO<sub>2</sub> measurements on commercial flights between 30°N and 30°S to integrate the local effects in the tropics at a larger scale.

All the sensitivity tests can be used to provide an overall estimation of CO<sub>2</sub> net surface fluxes and errors at continental scale. For each region, overall flux is defined as the average of all inferred fluxes from inversion  $S_0$  to inversion  $S_{14}$ . Overall variance  $\sigma_{T,j}^2$  of each region  $j$  is defined as

$$\sigma_{T,j}^2 = \sigma_{\langle S_{n,j} \rangle - S_{0,j}}^2 + \langle \sigma_{F_{n,j}}^2 \rangle$$

where  $n$  is the number of the inversion (Table 1),  $S_0$  is our control inversion,  $\sigma_{\langle S_{n,j} \rangle - S_{0,j}}^2$  is the variance of the 14 differences between inferred flux  $S_{n,j}$  and  $S_{0,j}$  and  $\langle \sigma_{F_{n,j}}^2 \rangle$  is the mean value of the variances of the 14 sensitivity tests. Overall error  $\sigma_{T,\varphi}$  is accounting for major sources of uncertainties involved in the carbon cycle, including atmospheric transport. Table 6 shows the overall fluxes and errors for five continental and four ocean regions.

Considering the implications for the Northern Hemisphere land sink, it is interesting to focus the analysis on the overall values for the 15°N-90°N latitude band. Figure 5 plots the range of the inferred fluxes over North America, Europe, and north Asia for all the 16 inversions performed. Overall value of the flux and associated error is also added on figure 5. We find a net land uptake of  $-0.7 \pm 0.7$  Gt C yr<sup>-1</sup> for North America,  $-0.5 \pm 0.8$  Gt C yr<sup>-1</sup> for Europe, and  $-1.2 \pm 0.8$  Gt C yr<sup>-1</sup> for North Asia. One should

note that errors on these three fluxes depend both on a priori uncertainties on land fluxes (that are chosen fairly large) and on the uncertainties introduced by all the sensitivity tests. The overall values of net fluxes mainly confirms the  $S_0$  longitudinal partition of the continental sink of the Northern Hemisphere (2.4 Gt C yr<sup>-1</sup>), with 55% of the sink located over Asia, 30% over North America and 15% over Europe. However, one can notice that error bars remain large for most regions. These results can be considered as our present limited knowledge of CO<sub>2</sub> sources and sinks for continental and ocean basins scale.

## 6. Conclusion

In this paper we investigate the sensitivity of the net CO<sub>2</sub> fluxes inferred in our control inversion  $S_0$  (see B99) to the main components involved in the inverse calculation. The differences obtained between all tests that we realize give an overview of the performances and the limitations of our Bayesian inverse technique applied with large continental and ocean regions. The influences of the  $\delta^{13}\text{C}$  measurements, the initial error values, the initial flux values, the transport model, the a priori flux scenario, and the atmospheric network are studied and analyzed.

The main limitation is the lack of knowledge of the initial error of atmospheric transport. Changing from TM2 atmospheric transport model to the TM3 model causes the largest discrepancies between the different inversion results at all spatial scales. Other important limitations are the spatial patterns of a priori fluxes and the use of continental sites that are not well represented by the model. We show that some components such as the number of regions for which the fluxes are optimized or the initial error values set on these fluxes have some significant impact on the inferred fluxes in regions poorly constrained by the atmospheric measurements, such as the tropics. Nevertheless, Bayesian methodology provide a fairly stable evaluation of the CO<sub>2</sub> net surface fluxes (1) at a continental scale for temperate and boreal northern and southern hemispheres, (2) zonally in the tropics, and (3) with an overall reduction of a priori uncertainties.

Finally, an overall set of fluxes and errors for five continental regions and four ocean regions has been calculated accounting

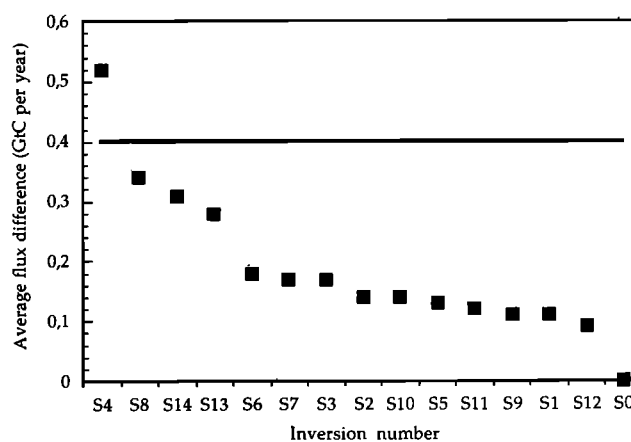


**Figure 4.** The  $\chi_m$  for all sensitivity study tests (in Gt C yr<sup>-1</sup>);  $\chi_m$  for test  $n$  is defined as the mean of the absolute differences between  $S_n$  and  $S_0$  inferred fluxes for the regions of Table 1. Tests are plotted following decreasing  $\chi_m$ . Solid line represents overall averaged a posteriori uncertainty at continental and ocean basins scale calculated as the mean uncertainty of the regions defined in Table 1.

**Table 6.** Overall Net Fluxes and Errors at Continental Scale and Ocean Basin Scale Accounting for All Sensitivity Tests

	Flux	Error
Land uptake		
North America	-0.7 ± 0.7	0.7
Europe	-0.5 ± 0.8	0.8
North Asia	-1.2 ± 0.8	0.8
South of 30°N	0.7 ± 1.1	1.1
Ocean uptake		
North Pacific	-0.2 ± 0.3	0.3
North Atlantic	-0.7 ± 0.3	0.3
15°N-15°S	0.5 ± 0.2	0.2
15°S-90°S	-1.0 ± 0.3	0.3

In Gt C yr<sup>-1</sup>. For each superregion, "flux" is the average of all optimized sources and sinks ( $S_1$  to  $S_{14}$ ). Total variance (square of "error") is defined in the text.

for all tests performed. By so doing, we obtain for the controversial partition of the CO<sub>2</sub> uptake at mid north latitudes:  $-0.7 \pm 0.7$  Gt C yr<sup>-1</sup> for North America,  $-0.2 \pm 0.3$  Gt C yr<sup>-1</sup> for North Pacific Ocean,  $-0.5 \pm 0.8$  Gt C yr<sup>-1</sup> for Europe,  $-0.7 \pm 0.3$  Gt C yr<sup>-1</sup> for North Atlantic Ocean, and  $-1.2 \pm 0.8$  Gt C yr<sup>-1</sup> for north Asia.

A lot of work remains to be done in the field of inverse calculation of CO<sub>2</sub> fluxes. The use of transport models with a higher resolution (both horizontally and vertically), which could better represent continental stations, is one issue for the next few years. In this context, the TRANSCOM III experiment is a first step toward the solution of this problem [Denning et al., 1997]. The decrease of the time resolution of the inferred fluxes from annual means to monthly means is an important step that has already been accomplished in several groups around the world [Rayner et al., 1997; Kaminski et al., 1997; Peylin et al., 1999]. The introduction of spatial and temporal correlations between sources is an other point that should be addressed in the near future. This would have the advantage of adding more constraints to the fluxes and thus would stabilize the solution when using a large number of source base functions. This task could be performed using the outputs of interannual biospheric and ocean 3-D models. Finally, addressing the interannual variability of CO<sub>2</sub> fluxes using inverse methods is an issue that should very soon be under the scope of the CO<sub>2</sub> community.

### Appendix: Including $\delta^{13}\text{C}$ Measurements in the Inversion

Potentially, the isotope ratio  $^{13}\text{C}/^{12}\text{C}$  of atmospheric CO<sub>2</sub> makes it possible to determine the global partitioning between land and ocean. This is because plant photosynthesis discriminates against  $^{13}\text{C}$ , whereas the dissolution of CO<sub>2</sub> in the sea waters proceeds with a small fractionation. As a result, plant tissues are depleted in  $^{13}\text{C}$  compared to the atmosphere and a global net storage in terrestrial ecosystems translates into an enrichment of  $^{13}\text{C}$  in the atmosphere [Ciais et al., 1995a].

#### A1. Method

In order to use  $\delta^{13}\text{C}$  measurements to constrain CO<sub>2</sub> fluxes, we must express  $\delta^{13}\text{C}$  as a function of modeled responses  $\chi_j$  of

the CO<sub>2</sub> source base functions  $F_j$  [see Bousquet et al, this issue, section 2]. Using the formulation of [Ciais et al., 1995a; Hein et al., 1997; Tans et al., 1993] one can write at a given point of the atmosphere where a source or a sink is present :

$$\frac{d[\rho\chi(\delta_a - \bar{\delta}_a)]}{dt} = (\delta_f - \bar{\delta}_a)F_{\text{fos}} + (\delta_d - \bar{\delta}_a)F_{\text{def}} + \varepsilon_{\text{ph}}F_{\text{b}} + \varepsilon_{\text{ao}}F_{\text{o}} + (\delta_{\text{ae}}^{\text{b}} - \bar{\delta}_a)F_{\text{soil}} + (\delta_{\text{ae}}^{\text{o}} - \bar{\delta}_a)F_{\text{oa}} \quad (\text{A1})$$

with  $\bar{\delta}_a$  mean  $\delta^{13}\text{C}$  of the atmosphere (-8‰);  
 $\bar{\chi}_a$  mean CO<sub>2</sub> concentration in the atmosphere (350 ppmv);  
 $\delta_a$  modeled  $\delta^{13}\text{C}$  in the atmosphere;  
 $\chi$  CO<sub>2</sub> mixing ratio;  
 $F_{\text{fos}}$  net CO<sub>2</sub> fossil fuel emissions;  
 $\delta_f$   $\delta^{13}\text{C}$  of fossil fuel CO<sub>2</sub>;  
 $F_{\text{d}}$  net CO<sub>2</sub> deforestation emissions;  
 $\delta_d$   $\delta^{13}\text{C}$  of deforested CO<sub>2</sub>;

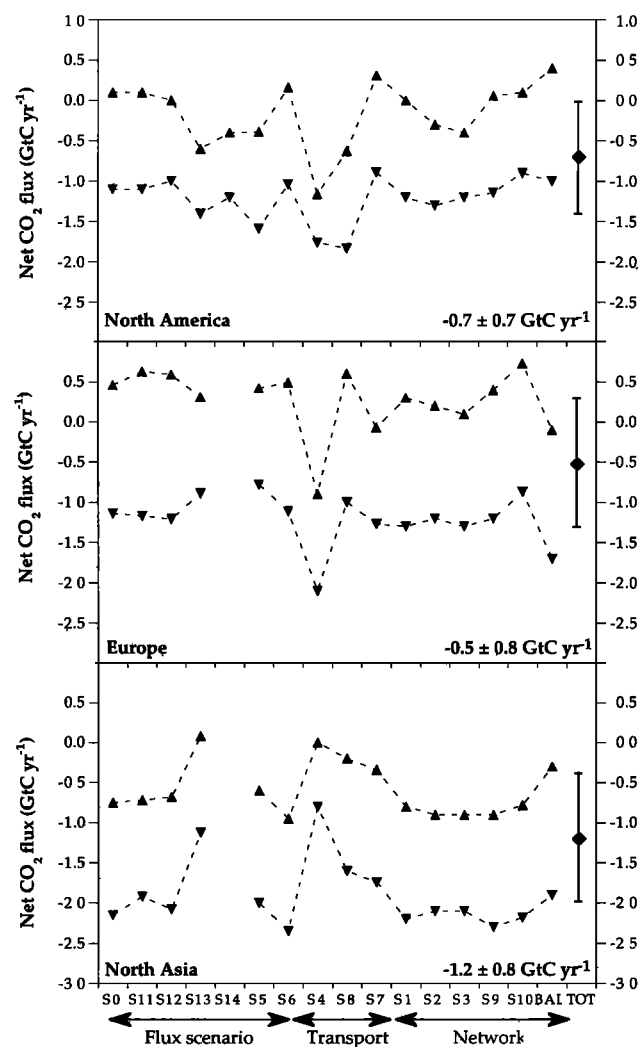


**Figure 5.** Optimized uptakes for three continental regions: North America, Europe, and north Asia. All sensitivity tests are plotted from  $S_0$  to  $S_{14}$  together with overall value of uptake and error (column TOT) as explained in the text.  $S_{14}$  is not available for Europe and north Asia separately because they are regrouped in this test.

$\epsilon_{\text{ph}}$	discrimination of terrestrial photosynthesis;
$F_b$	Net ecosystem production (GPP + RES);
$\epsilon_{\text{ao}}$	discrimination associated to <sup>13</sup> CO <sub>2</sub> dissolution in sea waters;
$F_o$	net air/sea exchange flux;
$F_{\text{soil}}$	soil respiration;
$\delta_{ae}^b - \delta_a$	disequilibrium terrestrial biosphere and atmosphere;
$F_{\text{oa}}$	gross ocean to atmosphere exchange flux;
$\delta_{ae}^o - \delta_a$	disequilibrium ocean surface and atmosphere;

All these variables except  $\bar{\chi}_a$  and  $\delta_a$  depend on both space and time ( $x, t$ ). In order to simplify notation this dependence will not be mentioned explicitly. This global equation of the  $\delta^{13}\text{C}$  budget has terms proportional to the net CO<sub>2</sub> fluxes ( $F_{\text{fos}}$ ,  $F_{\text{def}}$ ,  $F_b$ , and  $F_o$ ) and to the isotopic delta of the flux that we call equilibrium isotopic signature ( $\Delta_j$ ). Equation (A1) has also two disequilibrium terms which represent net fluxes of  $\delta^{13}\text{C}$  with no counterparts in net CO<sub>2</sub> fluxes. The isotopic disequilibria of the ocean and of the land biota are proportional to a gross CO<sub>2</sub> exchange flux and to an isotopic imbalance that we call disequilibrium isotopic signature ( $\Delta_j^d$ ). Thus derivative of  $\delta^{13}\text{C}$  is expressed as a linear combination of CO<sub>2</sub> net fluxes plus two disequilibrium terms which are specific to  $\delta^{13}\text{C}$ . Assuming that  $\chi \approx \bar{\chi}_a$  for CO<sub>2</sub>, equation (A1) can be rewritten as

$$\frac{d[\rho(\delta_a - \bar{\delta}_a)]}{dt} = \sum_{j=1}^{N_s} \frac{m_j \Delta_j}{\bar{\chi}_a} \hat{f}_j + \sum_{j=1}^{N_d} \frac{m_j^d \Delta_j^d}{\bar{\chi}_a} \hat{f}_j^d \quad (\text{A2})$$

where  $N_s$  is the number of sources related to CO<sub>2</sub> net fluxes and  $N_d^d$  is the number of disequilibrium terms.  $\hat{f}_j$  represents normalized CO<sub>2</sub> source base functions associated to variables  $m_j$  (source strengths) and  $\Delta_j$  (equilibrium isotopic signature), and  $\hat{f}_j^d$  represents normalized source base functions for disequilibrium terms (CO<sub>2</sub> gross fluxes) associated to variables  $m_j^d$  (gross fluxes strengths) and  $\Delta_j^d$  (disequilibrium isotopic signature). To solve equation (A2) we run the atmospheric transport model for CO<sub>2</sub> source base functions  $\hat{f}_j$  (already done for control inversion), and additionally, we run source base functions for disequilibrium terms  $\hat{f}_j^d$ . By doing so,  $\delta_a$  can be expressed as a combination of the modeled responses  $\hat{\chi}_j$  of normalized CO<sub>2</sub> source base functions and of the modeled responses  $\hat{\chi}_j^d$  of normalized source base functions for the CO<sub>2</sub> gross fluxes:

$$\delta_a - \bar{\delta}_a = \sum_{j=1}^{N_s} \frac{m_j \Delta_j}{\bar{\chi}_a} \hat{\chi}_j + \sum_{j=1}^{N_d} \frac{m_j^d \Delta_j^d}{\bar{\chi}_a} \hat{\chi}_j^d = g(\mathbf{m}, \Delta) \quad (\text{A3})$$

Function  $g$  is no more linear in  $\mathbf{m}$  but in  $\mathbf{m}\Delta$ . In the following, the quantity  $\mathbf{m}\Delta$  is called an "isoflux". A priori values for  $m_j$ ,  $\Delta_j$  and isoflux  $m_j \Delta_j$  are given in Table A1. We see that the strong negative isoflux imposed by anthropogenic emissions is not compensated by a priori values of other isofluxes. This means that inversion has to adjust positive isofluxes in order to close  $\delta^{13}\text{C}$  budget.  $S_0$ , the three processes that should be modified are the net exchange with land biota and the two disequilibrium terms. Net ocean contribution should not be influenced as it remains one order of magnitude lower than others due to the small discrimination associated with air-to-sea exchange.

The  $\delta^{13}\text{C}$  data provide constraints on the CO<sub>2</sub> net fluxes but also add new parameters to optimize: the CO<sub>2</sub> gross fluxes and

**Table A1.** Isotopic Signatures and Isofluxes for Different Processes Involved in <sup>13</sup>CO<sub>2</sub> Atmospheric Budget

Parameter	Value, ‰	Flux, Gt C yr <sup>-1</sup>	Isoflux, ‰ Gt C yr <sup>-1</sup>	Trend
$\delta_{\text{atm}}$ (1990)	-7.76	-	-	-
$\delta_f$	-28.4 *	5.9	-120.4	-0.160
$\delta_d$	-27	1.6	-43.2	-0.057
$\epsilon_{\text{ph}}$	-18	-1.8	32.4	0.040
$\epsilon_{\text{ao}}$	-2	-2	4	0.005
$\delta_{ae}^b - \delta_a$	0.2	60	12	0.020
$\delta_{ae}^o - \delta_a$	0.43	90	38.7	0.040

Isotopic signatures are from *Tans et al.* [1993]. Contribution to global trend has been calculated by dividing isoflux by atmospheric mean CO<sub>2</sub> concentration and by conversion factor  $f$  from ppmv to Gt C yr<sup>-1</sup> ( $f=2.122$ ).

\* From *Andres et al.* [1993].

the isotopic signatures. In order to reduce total degrees of freedom, soil respiration flux  $F_{\text{soil}}$  (part of terrestrial disequilibrium) is optimized together with total respiration using [*Lloyd and Farquhar*, 1994] coefficient  $\Phi$  to link soil respiration to total respiration as

$$F_{\text{soil}} = (1 - \Phi) F_{\text{resp}} \quad (\text{A4})$$

As for CO<sub>2</sub>, we add a global offset to  $g$  to account for the baseline  $\delta^{13}\text{C}$  of the atmosphere without sources. We also add  $\delta^{13}\text{C}$  global trend as an additional constrain on the global  $\delta^{13}\text{C}$  budget. In summary, with both  $\delta^{13}\text{C}$  and CO<sub>2</sub> atmospheric data we optimize CO<sub>2</sub> net fluxes, CO<sub>2</sub> gross air/sea exchange, and all isotopic signatures associated with these fluxes.

In order to solve practically the inverse problem for  $\delta^{13}\text{C}$  one possible way is to linearize equation (A3) around a priori  $\mathbf{m}_p$  and  $\Delta_p$  values. Introducing vector

$$\mathbf{m}_T: \mathbf{m}_T = \begin{pmatrix} \mathbf{m} \\ \Delta \end{pmatrix}$$

one can write

$$g(\mathbf{m}_T) = g(\mathbf{m}_{T_p}) + G_0(\mathbf{m}_T - \mathbf{m}_{T_p}) \quad (\text{A5})$$

**Table A2.** Anthropogenic Regions and Fluxes Used by the Inversion

	Flux	Error	$\Delta$	Error
Global fossil fuels	5.9	0.3	-20.4	1.0
American deforestation	0.6	0.6	-20.0	1.0
Africa deforestation	0.4	0.4	-20.0	1.0
Asia deforestation	0.6	0.6	-15.0	1.0

In Gt C yr<sup>-1</sup>.

**Table A3.** Land Regions Used for the Inversion

Land Region	GPP Flux	Error	Net Uptake	Error	$\Delta$	Error
North of 70°N	0.9	0.6	0.0	0.5	-17.2	-1.0
Boreal North America	5.3	2.8	0.0	1.5	-18.0	-1.0
Boreal Europe	2.6	1.7	0.0	1.5	-18.5	-1.0
Boreal Asia	4.6	3.2	0.0	1.5	-18.7	-1.0
Temperate North America	5.9	3.0	0.0	1.5	-18.6	-1.0
Temperate Europe	5.2	3.5	0.0	1.5	-18.8	-1.0
Temperate Asia	4.9	3.3	0.0	1.0	-20.0	-1.0
Trop. South America	24.3	11.0	0.0	1.0	-18.0	-1.0
Tropical Africa	5.2	6.3	0.0	1.0	-16.7	-1.0
Tropical Asia	8.8	4.9	0.0	1.0	-15.0	-1.0
South of 30°S	21.6	10.3	0.0	1.0	-15.4	-1.0
Total	100.0	20.0	-2.0	4.0	-	-

Annual gross and net biotic fluxes isotopic signature and errors used as a first guess in the inversion. Gross fluxes spatiotemporal patterns are given by *Denning et al.* [1996]. Net fluxes spatial patterns are given by *Friedlingstein et al.* [1995]. Fluxes and errors are expressed in Gt C yr<sup>-1</sup>.

with

$$(\mathbf{G}_0)_{i,j} = \left( \frac{\partial g_{i,j}}{\partial m_{T_i}} \right)_{\mathbf{m}_T = \mathbf{m}_{T_p}} \quad (\text{A6})$$

In these conditions, according to *Tarantola* [1987] and the formalism described by *Bousquet et al.* [this issue, section 2] the maximum likelihood solution can be expressed as

$$\langle \mathbf{m}_T \rangle = \mathbf{m}_{T_p} + \left( \mathbf{G}_0^t \mathbf{C}_d^{-1} \mathbf{G}_0 + \mathbf{C}_m^{-1} \right)^{-1} \mathbf{G}_0^t \mathbf{C}_d^{-1} [\mathbf{d}_{\text{obs}} - \mathbf{g}(\mathbf{m}_{T_p})] \quad (\text{A7})$$

This solution is close to the solution found for CO<sub>2</sub> (see section 2 of B99) but differs in the construction of matrix  $\mathbf{G}_0$  and in the fact that  $\mathbf{g}(\mathbf{m}_{T_p})$  must be calculated explicitly. A posteriori covariance matrix  $\mathbf{C}'_m$  is thus

$$\mathbf{C}'_m = \left( \mathbf{G}_0^t \mathbf{C}_d^{-1} \mathbf{G}_0 + \mathbf{C}_m^{-1} \right)^{-1} \quad (\text{A8})$$

As we linearize around the a priori conditions, it is not necessary to perform several iterations. An other possibility

would be to linearize around the maximum likelihood point. This approach can be very important for highly nonlinear problems, which is not the case for  $\delta^{13}\text{C}$  in CO<sub>2</sub>. Including  $\delta^{13}\text{C}$  data in the inversion increases the number of constraints by 25% (1000 to 1300) and the number of parameters to optimize by 100% (40 to 80). So the typical size of the matrix to inverse is now 80 columns and 1300 lines. The problem is still largely overconstrained.

## A2. Atmospheric Data

For  $\delta^{13}\text{C}$  data we use 24 time series provided by the NOAA CMDL flask network [*Trolier et al.*, 1996]. Isotopic data have been measured since the early 1990s. These data are smoothed within the time domain using exactly the same procedure as for CO<sub>2</sub> data [*Thoning et al.*, 1989]. However,  $\delta^{13}\text{C}$  data are not extrapolated beyond the measured time domain.

## A3. A Priori Flux Scenario

Practically,  $\delta^{13}\text{C}$  in the atmosphere is expressed as the sum of isofluxes for all CO<sub>2</sub> sources and sinks, plus two desequilibrium terms. Thus all the CO<sub>2</sub> source base functions calculated by *Bousquet et al.* [this issue] can be used for nondesequilibrium terms. Desequilibrium with lands is linked to total respiration via the coefficient of *Lloyd and Farquhar* [1994] as explained

**Table A4.** Oceanic Regions Used for the Inversion

Oceanic regions	Net Flux	Error	$\Delta$	Error	Gross Flux	Error	$\Delta$	Error
Austral ocean	-0.3	1.5	-2.0	0.5	20.5	8.2	-0.5	0.2
20°S-50°S oceans	-0.8	1.5	-2.0	0.5	24.8	6.0	0.6	0.2
Tropical oceans	0.8	1.5	-2.0	0.5	19.0	7.6	1.6	0.2
North Pacific 15-45° N	-0.2	1.0	-2.0	0.5	7.0	4.2	0.3	0.2
North Pacific 45-60°N	-0.1	1.0	-2.0	0.5	3.5	4.2	-0.5	0.2
North Atlantic 15-50°N	-0.3	1.0	-2.0	0.5	5.5	2.2	0.7	0.2
North Atlantic - 50-80°N	-0.4	1.0	-2.0	0.5	4.2	1.7	-0.9	0.2
North of 60°N (not Atlantic)	-0.0	1.0	-2.0	0.5	2.1	0.8	-1.0	0.2
Total	-1.2	3.0	-	-	86.5	15.0	-	-

Annual net oceanic fluxes and errors used as a first guess in the inversion. Net fluxes spatiotemporal patterns are given by *Takahashi et al.* (1997). Fluxes and errors are expressed in Gt C yr<sup>-1</sup>.

previously and does not imply the running of additional base functions. However, eight specific source base functions are run to account for gross ocean exchange.

**A3.1. Land fluxes.** The  $\delta^{13}\text{C}$  of all fossil fuels is set to  $\delta_f = -28.4 \pm 1\%$  [Andres *et al.*, 1993]. Table A2 summarizes these figures. We use the work of Ciais *et al.* [1995a] to evaluate a spatial distribution of the discrimination  $\epsilon_{\text{ph}}$  and of the isotopic disequilibrium term  $\delta_{\text{ae}}^{\text{b}} - \delta_a$ . A value of  $\epsilon_{\text{ph}}$  of  $-15\%$  has been arbitrarily given to SIB2 biomes dominated by C<sub>4</sub> plants [Ciais *et al.*, 1995a]. Determination of  $\delta_{\text{ae}}^{\text{b}} - \delta_a$  is based on CENTURY model [Schimel *et al.*, 1994] modified by [Ciais *et al.*, 1998]. The  $\delta^{13}\text{C}$  of deforested CO<sub>2</sub> has been taken to be  $-20\%$  except in Asia where a priori value is  $-15\%$  according to C<sub>4</sub> plants proportions in this region. All isotopic signatures are listed in Table A3. Errors are fixed at 1‰ for equilibrium signatures and at 0.2‰ for disequilibrium ones.

**A3.2. Ocean fluxes.** Isotopic signatures of net air-sea exchanges are based on work by Tans *et al.* [1993] for the spatial distribution of  $\epsilon_{\text{ao}}$  and  $\delta_{\text{ae}}^{\text{o}} - \delta_a$ . Errors are set to 1‰ for  $\delta^{13}\text{C}$  equilibrium signatures and at 0.2‰ for  $\delta^{13}\text{C}$  disequilibrium ones. Gross flux  $F_{\text{oa}}$  is built as the product of the exchange coefficient calculated to evaluate net flux  $F_0$  and a constant value of 340 ppmv as in Enting *et al.* [1993]. Global value of  $F_{\text{oa}}$  is 86.5 Gt C yr<sup>-1</sup> (Table A4). It is important to note that this parametrization of  $\delta^{13}\text{C}$  in dissolved inorganic carbon (DIC) is coarse as it may depend on latitude and on time. One may expect  $\delta^{13}\text{C}$  to be strongly influenced by biology and to a certain extent by the supply of  $\delta^{13}\text{C}$  from bottom waters rich in nutrients and remineralized carbon.

**Acknowledgments.** M. Heimann (MPI - Iena) is to be thanked for providing LSCE with both TM2 and TM3 models. The authors thank Peter Rayner for fruitful discussions about inversion method. This work is supported by the Programme National d'Etude de la Dynamique du Climat (PNEDC) and the Commission of the European Community under contracts ENV4CT95 and ENV4-Euro-Siberian Carbon Flux. Computing support was provided by Commissariat à l'Energie Atomique (CEA). This is contribution 155 of the LSCE.

## References

- Andres, R. J., G. Marland, T. Boden, and S. Bishoff, Carbon dioxide emissions from fossil fuel combustion and cement manufacture 1751-1991 and an estimate of their isotopic composition and latitudinal distribution, in *The Carbon Cycle*, edited by T.M. Wigley, p23-32, Cambridge Univ. Press, New York, 1993.
- Andrie, C., C. Oudot, C. Genthon, and L. Merlivat, CO<sub>2</sub> fluxes in the tropical Atlantic during FOCAL cruises, *J. Geophys. Res.*, **91**(C10), 11,741-11,755, 1986.
- Aumont, O., Etude du cycle naturel du carbone dans un modele tridimensionnel de l'océan mondial, Ph.D. thesis, Univ. Paris VI, Paris, 1998.
- Bousquet, P., P. Ciais, P. Monfray, Y. Balkanski, M. Ramonet, and P. Tans, Influence of two atmospheric transport models in inferring sources and sinks of atmospheric CO<sub>2</sub>, *Tellus, Ser. B*, **48**, 568-582, 1996.
- Bousquet, P., P. Ciais, P. Peylin, M. Ramonet, and P. Monfray, Inverse modelling of annual atmospheric CO<sub>2</sub> sources and sinks, 1, Method and control inversion, *J. Geophys. Res.*, *this issue*.
- Boutin, J., and J. Etcheto, Long-term variability of the air-sea CO<sub>2</sub> exchange coefficient: Consequences for the CO<sub>2</sub> fluxes in the equatorial Pacific Ocean, *Global Biogeochem. Cycles*, **11**(3), 453-470, 1997.
- Ciais, P., P.P. Tans, M. Trolier, J.W. White, and R. Francey, A large Northern Hemisphere terrestrial CO<sub>2</sub> sink indicated by the <sup>13</sup>C/<sup>12</sup>C ratio of atmospheric CO<sub>2</sub>, *Science*, **269**, 1098-1102, 1995a.
- Ciais, P., P.P. Tans, J.W. White, M. Trolier, R. Francey, J.A. Berry, D. Randall, P.J. Sellers, J.G. Collatz, and D.S. Schimel, Partitioning of ocean and land uptake of CO<sub>2</sub> as inferred by  $\delta^{13}\text{C}$  measurements from the NOAA Climate Monitoring and Diagnostic Laboratory global air sampling network, *J. Geophys. Res.*, **100**(D3), 5051-5070, 1995b.
- Ciais, P., P. Friedlingstein, D.S. Schimel, and P.P. Tans, A global calculation of the  $\delta^{13}\text{C}$  of soil respired carbon: Implications for the biospheric uptake of anthropogenic CO<sub>2</sub>, *Global Biogeochem. Cycles*, **13**(2), 519-530, 1999.
- Delecluse, P., M. Imbard, C. Lévy, and G. Madec, OPA-Ocean General Circulation model, LODYC report, Univ. Paris VI, Paris, 1993.
- Denning, A.S., I.Y. Fung, and D.A. Randall, Latitudinal gradient of atmospheric CO<sub>2</sub> due to seasonal exchange with land biota, *Nature*, **376**, 240-243, 1995.
- Denning, A.S., G. J. Collatz, C. Zhang, D. A. Randall, J. A. Berry, P. J. Sellers, G. D. Colello, and D. A. Dazlich, Simulation of terrestrial carbon metabolism and atmospheric CO<sub>2</sub> in a general circulation model, Part 1: Surface carbon fluxes, *Tellus*, **48B**, 521-542, 1996.
- Denning, A.S., et al., Intercomparison and calibration of global tracer transport simulations of SF<sub>6</sub>, paper presented at Fifth International Carbon Dioxide Conference, Commonwealth Sci. and Ind. Res. Org., Cairns, Australia, 1997.
- Enting, I.G., C.M. Trudinger, R.J. Francey, and H. Granek, Synthesis inversion of atmospheric CO<sub>2</sub> using the GISS tracer transport model, *Aust. Div. Atmos. Res. Tech. Pap., CSIRO*, **29**, 1-44, 1993.
- Enting, I.G., C.M. Trudinger, and R.J. Francey, A synthesis inversion of the concentration of  $\delta^{13}\text{C}$  of atmospheric CO<sub>2</sub>, *Tellus, Ser. B*, **47**, 35-51, 1995.
- Fan, S.-M., M. Gloor, J. Mahlman, S. Pacala, J.L. Sarmiento, T. Takahashi, and P.P. Tans, A large terrestrial carbon sink in North America implied by atmospheric and oceanic carbon dioxide data and models, *Science*, **282**, 442-446, 1998.
- Francey, R.J., P.P. Tans, C.E. Allison, I.G. Enting, J.W.C. White, and M. Trolier, Changes in oceanic and carbon uptake since 1982, *Nature*, **373**, 326-330, 1995.
- Friedlingstein, P., I. Fing, E. Holland, J. John, G. Brasseur, D. Erickson, and D. Schimel, On the contribution of CO<sub>2</sub> fertilization to the missing biospheric sink, *Global Biogeochem. Cycles*, **9**, 541-556, 1995.
- Heimann, M., The global atmospheric tracer model TM2, report, Max Planck Inst. für Meteorol., Hamburg, Germany, 1995.
- Heimann, M., and C.D. Keeling, A three-dimensional model of atmospheric CO<sub>2</sub> transport based on observed winds, 2, Model description and simulated tracer experiments, in *Aspects of Climate Variability in the Pacific and the Western Americas*, *Geophys. Monogr. Ser.*, vol 55, edited by D.H. Peterson, pp. 237-275, AGU, Washington, D.C., 1989.
- Hein, R., P.J. Crutzen, and M. Heimann, An inverse modeling approach to investigate the global atmospheric methane cycle, *Global Biogeochem. Cycles*, **11**(1), 43-76, 1997.
- Kaminski, T., M. Heimann, and R. Giering, A global scale inversion of the transport of CO<sub>2</sub> based on a matrix representation of an atmospheric transport model derived by its adjoint, paper presented at Fifth International Carbon Dioxide Conference, Commonwealth Sci. and Ind. Res. Org., Cairns, Australia, 1997.
- Keeling, R.F., S.C. Piper, and M. Heimann, Global and hemispheric CO<sub>2</sub> sinks deduced from changes in atmospheric O<sub>2</sub> concentration, *Nature*, **381**, 218-221, 1996.
- Law, R.M., CO<sub>2</sub> sources from a mass-balance inversion: Sensitivity to the surface constraint, paper presented at Fifth International Carbon Dioxide Conference, Commonwealth Sci. and Ind. Res. Org., Cairns, Australia, 1997.
- Law, R.M., et al., Variations in modeled atmospheric transport of carbon dioxide and the consequences for CO<sub>2</sub> inversions, *Global Biogeochem. Cycles*, **10**, 783-796, 1996.
- Lefèvre, N., A first step toward a reference DPCO<sub>2</sub> map for the North Atlantic Ocean, Int Geosphere-Biosphere Programme, Data and Inf. Syst., Lab d'Océanogr. Dyn. et de Climatol., Univ. Pierre et Marie Curie, Paris, 1995.
- Lloyd, J., and G.D. Farquhar, <sup>13</sup>C discrimination during CO<sub>2</sub> assimilation by the terrestrial biosphere, *Oecologia*, **99**, 201-215, 1994.
- Metzl, N., A. Poisson, F. Louanchi, C. Brunet, B. Schauer, and B. Bres, Spatio-temporal distributions of air-sea fluxes of CO<sub>2</sub> in the Indian and Antarctic Oceans: A first step, *Tellus, Ser. B*, **47**, 56-59, 1995.
- Monfray, P., M. Ramonet, and D. Beardsmore, Longitudinal and vertical CO<sub>2</sub> gradients over the subtropical/subantarctic oceanic sink, *Tellus, Ser. B*, **48**, 445-456, 1996.
- Peylin, P., P. Bousquet, P. Ciais, and P. Monfray, Time-Dependant versus Time-Independent inversion of the atmospheric CO<sub>2</sub> observations: Consequences for the regional fluxes, AGU, Washington DC, *Geophysical Monograph Series*, in press, 1999.

- Ramonet, M., and P. Monfray, CO<sub>2</sub> Baseline concept in 3-D atmospheric transport models, *Tellus, Ser. B*, 48, 502-520, 1996.
- Rayner, P., I. Enting, R. Francey, and R. Langenfelds, The recent time history of regional carbon sources as deduced from carbon dioxide and oxygen concentration and isotopic composition measurements, paper presented at Fifth International Carbon Dioxide Conference, Commonwealth Sci. and Ind. Res. Org., Cairns, Australia, 1997.
- Schimmel, D.S., B.H. Braswell, E.A. Holland, R. McKeown, D.S. Ojima, T.H. Painter, W.J. Parton, and A.R. Townsend, Climatic, edaphic, and biotic controls over storage and turnover of carbon in soils, *Global Biogeochem. Cycles*, 8(3), 279-293, 1994.
- Six, K.D., and E. Maier-Reimer, Effects of plankton dynamics on seasonal carbon fluxes in an ocean general circulation model, *Global Biogeochem. Cycles*, 10(4), 559-583, 1996.
- Sugawara, S., T. Nakazawa, S. Aoki, S. Morimoto, M. Toi, S. Yoshimura, and M. Tanaka, Variations of the CO<sub>2</sub> concentration and its carbon and oxygen isotopic ratios in the troposphere over Japan, paper presented at Fifth International Carbon Dioxide Conference, Commonwealth Sci. and Ind. Res. Org., Cairns, Australia, 1997.
- Takahashi, T., R.A. Feely, R. Weiss, R.H. Wanninkhof, D.W. Chipman, S.C. Sutherland, and T.T. Takahashi, Global air-sea flux of CO<sub>2</sub>: An estimate based on measurements of sea-air pCO<sub>2</sub> difference, *Proc. Natl. Acad. Sci., U.S.A.*, 94, 8292-8299, 1997.
- Tans, P.P., J.A. Berry, and R.F. Keeling, Oceanic <sup>13</sup>C/<sup>12</sup>C observations: A new window on ocean CO<sub>2</sub> uptake, *Global Biogeochem. Cycles*, 7(2), 353-368, 1993.
- Tarantola, A., *Inverse Problem Theory*, Elsevier, New York, 1987.
- Thoning, K.W., P.P. Tans, and W.D. Komhyr, Atmospheric carbon dioxide at Mauna Loa Observatory, 2, Analysis of the NOAA GMCC data, 1974, 1985, *J. Geophys. Res.*, 94(D6), 8549-8565, 1989.
- Trolier, M., J.W.C. White, P.P. Tans, K.A. Masarie, and P.A. Gemery, Monitoring the isotopic composition of atmospheric CO<sub>2</sub>: Measurements from the NOAA global air sampling network, *J. Geophys. Res.*, 101(D20), 25,897-25,916, 1996.
- 
- P. Bousquet, P. Ciais, P. Monfray, P. Peylin, and M. Ramonet, UMR CNRS/CEA, CEA de Saclay, Orme des Merisiers, Bat. 709/LSCE, Gif sur Yvette cedex, F-91191, France. (bousquet@lsce.saclay.cea.fr)
- (Received November 2, 1998; revised May 14, 1999; accepted May 19, 1999 )